OXYGEN ELECTRODE IN MOLTEN CARBONATE FUEL CELLS

(CONTRACT NUMBER: DE-FG22-87PC79931)

DOE/PC/79931--T6

DE91 005743

Twelfth Quarterly Technical Progress Report

(May 1, 1990 - July 31, 1990)

PERSONNEL:

Bhasker B. Davé*, Supramaniam Srinivasan

Ralph E. White*, and A. John Appleby

Center for Electrochemical Systems and Hydrogen Research

Texas Engineering Experiment Station

238 Wisenbaker Engineering Research Center

Texas A&M University System

College Station, Texas 77843

*** Department of Chemical Engineering, Texas A&M University**

College Station, Texas 77843

Sponsored by the U. S. Department of Energy

Pittsburgh Energy Technology Center

Abstract

During this quarter, impedance data were analyzed for oxygen reduction process in molten carbonate electrolyte and a manuscript,"Impedance Analysis for Oxygen Reduction in a Lithium Carbonate Melt: Effects of Partial Pressure of Carbon Dioxide and Temperature," was prepared which will be submitted to *Journal of the Electrochemical Society* for publication.

OXYGEN ELECTRODE IN MOLTEN CARBONATE FUEL CELLS

Introduction

This project focuses on three area of research:

Task 1: Construction of High Temperature Equipment

Task 2: Microelectrode Study of Oxygen Reduction

Task 3: Computer Modeling of Reactions

This report summarizes the work carried out during the last quarter (May 1, 1990 - July 31, 1990) and the work plan for the next quarter.

Work Carried Out During the Reporting Period

Task 2 : Microelectrode Study of Oxygen Reduction

During the last quarter, a paper on "Impedance Analysis for Oxygen Reduction in a Lithium Carbonate Melt: Effects of Partial Pressure of Carbon Dioxide and Temperature," was prepared which will be submitted for publication to *Journal of the Electrochemical Society* (Appendix A).

PROPOSED WORK DURING NEXT QUARTER

The research project will be completed by September 1990 and the final report will be prepared during the next quarter.

Appendix A

Impedance Analysis for Oxygen Reduction in a Lithium Carbonate Melt: Effects of Partial Pressure of Carbon Dioxide and Temperature

Bhasker B. Davé and Ralph E. White

Center for Electrochemical Engineering

Department of Chemical Engineering

Supramaniam Srinivasan and A. John Appleby

Center for Electrochemical Systems and Hydrogen Research

Texas A&M University

College Station, Texas 77843

Submitted as a Technical Paper

to the Editor

Journal of the Electrochemical Society

10 South Main street

Pennington, New Jersey 08534

December 1990

Key words: Electrochemical impedance spectroscopy, molten lithium carbonate, and oxygen reduction

Abstract

Effects of partial pressure of carbon dioxide and temperature on oxygen reduction kinetics in lithium carbonate melt were examined using electrochemical impedance spectroscopic (EIS) and linear sweep voltammetric techniques. The impedance spectra were analyzed by a Complex Nonlinear Least Square (CNLS) method, using the Randles-Ershler equivalent circuit model, to determine the electrode kinetic and the mass transfer parameters such as the charge transfer resistance and the Warburg coefficient. The cyclic voltammetric measurements indicated that the oxygen reduction process in lithium carbonate melt is "reversible" up to 200 mV/s. The product $D_O^{1/2}C_O$ determined by cyclic voltammetry agreed well with those estimated by the EIS method. The reaction order with respect to carbon dioxide and the activation energy for the exchange current density were determined to be -0.52 and 132 kJ/mol respectively. Also, the reaction order with respect to carbon dioxide and the activation energy for $D_O^{1/2}C_O$ were calculated to be -0.8 and 185 kJ/mol, respectively.

Introduction

The oxygen reduction reaction in molten alkali carbonate electrolytes has been studied for the past quarter century because of its vital role in the performance of the molten carbonate fuel cell. Borucka and Sugiyama (1,2) studied the $O_2/CO_2/Au$ electrode in a ternary (43.5 mol% Li : 31.5 mol% Na : 25.0 mol%)CO_3 eutectic melt in the temperature range of 550-800 °C and concluded the following: (i) the effects of the partial pressures of oxygen and carbon dioxide on the equilibrium potential show that the over-all reaction at equilibrium is

$$1/2O_2 + CO_2 + 2e^- \rightleftharpoons CO_3^{2-} \qquad [1]$$

and the equilibrium potential obeys the corresponding Nernst equation

$$E_{O_2,CO_2/CO_3^{2-}} = E^{\circ}_{O_2,CO_2/CO_3^{2-}} + \frac{RT}{2F}\ln\left(P_{O_2}^{1/2}P_{CO_2}\right); \qquad [2]$$

(ii) the micropolarization tests at near-equilibrium indicate that the electrode is under "mixed" control, due to the charge transfer and the mass transport processes, even close to the equilibrium; and (iii) the exchange density for the electrode reaction (Eqn. [1]) is about 0.1 mA cm^{-2}. Appleby and Nicholson (3-6) examined the oxygen reduction reaction in molten carbonates on a submerged gold electrode using steady-state and potential-scan techniques. They observed that oxygen reacts with carbonate ions and forms peroxide and/or superoxide ions and the concentrations of these species depend on the cations present in the melt. In a pure Li_2CO_3 or a Li-rich melt the peroxide species is dominant, whereas in a K-rich melt the superoxide species is dominant. They proposed the following reaction mechanism for oxygen reduction in pure lithium carbonate melt:

$$1/2O_2 + CO_3^{2-} \rightleftharpoons O_2^{2-} + CO_2 \qquad [3]$$

$$O_2^{2-} + e^- \rightleftharpoons (O^-) + O^{2-} \quad [4]$$

$$(O^-) + CO_2 + e^- \rightleftharpoons CO_3^{2-} \quad [5]$$

$$O^{2-} + CO_2 \rightleftharpoons CO_3^{2-} \quad [6]$$

$$1/2O_2 + CO_2 + 2e^- \rightleftharpoons CO_3^{2-} \quad [7]$$

where (O^-) is a transient species. According to this reaction mechanism, the first charge transfer reaction (Eqn. [4]) is the rate determining step for an immersed electrode. Appleby and Nicholson also examined the oxygen reduction in binary (47 mol% Li : 53 mol% K and 43 mol% Na : 57 mol% K) and ternary (43.5 mol% Li : 31.5 mol% Na : 25 mol% K) eutectics in the temperature range of 700-800 °C and concluded that: (i) the electroactive species is not the oxygen molecule; (ii) both peroxide and superoxide ions are present and are reduced in the parallel steps; and (iii) the neutralization of the oxide ions by carbon dioxide (Eqn. [6]) is slow. Andersen (7) carried out a thermodynamic study on the chemical equilibria in molten alkali carbonate electrolytes and demonstrated the presence of peroxide ions in quenching experiments followed by chemical analyses. Appleby and Van Drunen (8) determined the total solubility of oxygen (mainly in the form of peroxide and superoxide ions) in molten carbonate electrolytes as a function of temperature using quenching method. Vogel *et al.* (9) studied the (Li-K)CO_3 eutectic melt at 650 °C, using a rotating gold wire and concluded that superoxide is dominant in this melt and the concentration of molecular oxygen in the melt is negligible. Smith *et al.* (10) determined the total solubility of oxygen in (Li-Na-K)CO_3 eutectic melt as a function of gas composition at 650 °C, using a chemical method. They concluded that oxygen reacts with (Li-Na-K)CO_3 melt at 650 °C to form superoxide ions and the concentration of physically dissolved, molecular,

oxygen is negligible. Dunks and Stelman (11) studied the oxygen reduction in a pure sodium carbonate at 900 oC using cyclic voltammetric and computer-curve fitting and proposed the existence of percarbonate ions. They also confirmed the presence of superoxide ion in frozen electrolyte by Electron Spin Resonance (ESR) spectrum at 77 K. Lu (12) investigated the oxygen reduction process in pure Li_2CO_3 and a Li-K (62 mol%:38 mol%) carbonate eutectic mixture using a potential step method. The exchange current density, determined by Lu (39 mA/cm^2 for 90% O_2 and 10% CO_2 at 750 °C in Li_2CO_3 melt), is two orders of magnitude higher than that reported by Appleby and Nicholson (0.34 mA/cm^2) who used the potential scan technique. But the dependence of oxygen reduction kinetics on partial pressures of oxygen and carbon dioxide observed by Lu could not be explained by any of the mechanism proposed in the literature. Uchida *et al.* (13) determined the electrode kinetic parameters for oxygen reduction in a (Li-K)CO_3 (42.7 mol%:57.3 mol%) eutectic melt on a gold electrode using impedance analysis, potential step, and coulostatic relaxation techniques. They found that the exchange current density was about the same order of magnitude as that of Lu. In addition, they concluded that of the three methods for the determination of the electrode kinetic parameters for oxygen reduction in molten carbonates the impedance analysis is the most reliable. Uchida *et al.* (14) examined the oxygen reduction on a lithiated NiO film, deposited on gold, and Sb-doped SnO_2 electrodes in Li-K eutectic melt by impedance spectroscopy and coulostatic relaxation techniques. They (15) also determined the temperature dependence of the electrode kinetic and mass transfer related parameters for oxygen reduction on gold in (Li-K)CO_3. Adanuvor *et al.* (16) simulated the oxygen reduction reaction in various alkali carbonate melts; the mathematical model

considered the simultaneous presence of peroxide and superoxide ions with slow neutralization reaction. The simulation results indicate that the melts with high Li-content would favor the kinetic rates. Ramaswami (17) used a rotating disk electrode made of gold to study the oxygen reduction reaction in a pure lithium carbonate melt at 800 °C, and determined the diffusion coefficient and peroxide ion concentration as a function of partial pressure of oxygen.

The mechanism of oxygen reduction in molten carbonate is not well understood and the results reported in the literature are not consistent. Moreover, oxygen reduction in molten carbonate has fast kinetics, and even near-equilibrium tests reported in the literature indicate mixed-control kinetics. The previous studies show that the presence of physically dissolved molecular oxygen in molten carbonate electrolyte is insignificant. Oxygen reacts with the molten alkali carbonates to form peroxide and/or superoxide ions; the concentrations of these species depend on the cations present in the melt. Thermodynamic data (7) indicate that equilibrium concentration of the superoxide ion decreases with decrease in the ionic radii of the alkali cations, i.e. $C_{O_2^-}$ is in the order K > Na > Li), and in a pure lithium carbonate melt the superoxide ion is unstable. Consequently, in the present work, we have used pure lithium carbonate melt to avoid the complexity of simultaneous formation of peroxide and superoxide ions. In the previous work (17,18) we have reported the effects of partial pressure of oxygen and temperature on electrode kinetics and mass transfer parameters for oxygen reduction in pure lithium carbonate melt. In the present work the influence of partial pressure of carbon dioxide on the oxygen reduction kinetics was investigated by electrochemical impedance spectroscopy (EIS) and cyclic voltammetry. Also, the temperature dependence of oxygen reduction kinetic was examined.

Experimental

The experimental setup for high temperature electrode kinetic study and methodology are as described somewhere else (18). The working electrode was made of a submerged gold flag (0.025 mm thick), with a geometrical area of one square centimeter, connected to the gold current collector (0.5 mm diameter) by a thin gold wire to minimize the meniscus effect (2,17,19). The counter electrode was a large gold foil circumscribing the working electrode to ensure uniform current distribution. The reference electrode was also made of a gold foil, but encased in an alumina tube which was pressed against the bottom of the electrochemical cell. The high purity (99.9%) gold foils and wires were obtained from Johnson Matthey/ÆSAR Group.

Digital mass flow controllers/meters manufactured by Teledyne-Hastings Raydist were used to provide the gas mixtures of the desired compositions (O_2, CO_2 and Ar) with high precision (± 1% Full Scale). The high purity gases were obtained from Matheson Gas Products and the traces of water were removed by passing the blended gas through a column of 5 Å molecular sieves and Drierite (Fisher Scientific). The gas mixture was bubbled into the melt in the vicinity of the working electrode at a flow rate of 50 $cm^3\ min^{-1}$ through a long alumina tube with four holes. The composition of the gas mixture supplied to the reference electrode compartment was the same as the one used for the working electrode, but at a lower flow rate (5 $cm^3\ min^{-1}$). In this study, P_{CO_2} was varied from 0.02 to 0.4 atm., while P_{O_2} was maintained constant at 0.6 atm. The total pressure was 1 atm., by varying the partial pressure of argon. The high purity (99.999%) lithium carbonate (Alfa Products) was carefully weighed in an alumina crucible (90 ml capacity) and the electrochemical cell was slowly heated (50°C/hr) to

350°C in an inert environment. The electrochemical cell assembly was dried at 350°C in a carbon dioxide environment for 24 hours before heating to 800°C.

The data acquisition set-up consisting of a potentiostat/galvanostat (Model 273), lock-in-amplifier (Model 5301A), personal computer (IBM PS/2), and software (Model 378) supplied by EG&G Princeton Applied Research was used for the cyclic voltammetric and electrochemical impedance spectroscopic experiments. For the EIS, measurements were made over a wide range of frequencies (0.05 Hz to 10 kHz) for the sinusoidal excitation signal, because the capacitive effect, attributed to the double layer, is significant at high frequency, and the diffusional (Warburg) impedance is dominant at low frequency. The impedance measurements for frequencies higher than 5 Hz were carried out by the Phase Sensitive Detection (PSD) technique using the lock-in-amplifier and the potentiostat. For frequencies below 5 Hz, the cell impedance was measured by the Fast Fourier Transform (FFT) technique using, the personal computer and potentiostat. The results of low frequency measurements (below 5 Hz) represent the average values of 15 data cycles, which was done to improve the accuracy of the data by averaging out the noise interference. The amplitude of the excitation signal was kept at 5 mV to ensure a linear electrochemical response.

Results and Discussion

Impedance Measurements and Analyses

The impedance spectra were obtained for oxygen reduction on the submerged gold electrode in lithium carbonate melt at the equilibrium potential as a function of P_{CO_2} and temperature. As described in the previous work (17,18), the absence of a semicircle in the complex plane impedance plot indicated fast

oxygen reduction kinetics (20). In the region of low frequency, the complex plane plot showed a linear behavior with a slope of 45° due to the Warburg impedance (21). The effect of partial pressure of carbon dioxide on the Bode plot, phase angle vs. log ω, at 800°C is shown in Fig. 1. In a high frequency region, the phase angle approached 0° for all plots, indicating a purely resistive behavior of the cell impedance. The impedance at 0° phase angle is a measure of the uncompensated electrolyte resistance, R_s, between the working and the reference electrodes. At frequencies below 30 Hz, the phase angle approached −45°, indicating that the diffusional impedance is significant. The influence of partial pressure of carbon dioxide on oxygen reduction kinetics was evident at the intermediate frequencies, showing the increased charge transfer resistance with an increase in P_{CO_2}. The sharp deviations in the Bode plots at about 120 Hz (second harmonic frequency of the line) cannot be explained a this time.

The impedance spectra were resolved by using the Randles-Ershler equivalent circuit (22, 23) model shown in Fig. 2. The Randles-Ershler equivalent circuit reflects two parallel process occurring at the electrode-electrolyte interface, namely, the double layer charging and the faradaic reaction. The faradaic impedance consists of the charge transfer resistance which is in series with the Warburg (diffusional) impedance. The uncompensated electrolyte resistance between the working and reference electrodes, R_s, is connected in series with the interfacial impedance. A Complex Nonlinear Least Square (CNLS) parameter estimation program (24-26), based on Levenberg-Marquardt algorithm, was used to resolve the impedance spectra. In our analysis, we found that the weighting factor (inverse of the error variance) considerably influenced the accuracy of the parameters estimated from the impedance data (18). Here, we have used

the proportional and functional proportional weighting factors (27) to determine the electrode kinetic and the mass transfer parameters This analysis yields parameters such as the charge transfer resistance, double layer capacity, Warburg coefficient, and uncompensated electrolyte resistance. The parameter estimation by the complex nonlinear least square method also provides the standard deviation of the estimated parameters.

The influence of partial pressure of carbon dioxide on real part of impedance (Z') vs. inverse square root of angular frequency ($\omega^{-1/2}$) for 800 °C temperature is shown in Fig. 3. In a low frequency region, Z' vs. $\omega^{-1/2}$ plots showed a linear behavior with a slope proportional to the Warburg Coefficient (σ). As demonstrated in Fig. 3, the Warburg coefficient increased with an increase in P_{CO_2}, which was due to the decrease in the peroxide ion concentration (Eqn. [3]). As shown in Fig. 3, the model impedance data, calculated using the estimated parameters and the Randles-Ershler equivalent circuit model, agreed well with the experimental data. The electrode kinetic and mass transfer parameters as function of P_{CO_2} for temperatures 750, 800 and 850°C are presented in Tables 1-3 respectively. As shown in these tables, for a decrease in P_{CO_2} from 0.4 to 0.02 atm. caused a ten fold decrease in the magnitude of the Warburg coefficient. A similar trend was observed when temperature was increased from 750 to 850°C. The charge transfer resistance also decreased with an increase in temperature and a decrease in partial pressure of carbon dioxide. The double layer capacity observed for the smooth gold electrode in a pure lithium carbonate melt was much higher than that observed for a smooth electrode in an aqueous electrolytes. Also the double layer capacity increased with the decrease in P_{CO_2} and this increase was more significant at higher temperature. This dependence of capacity

on temperature and P_{CO_2} cannot be explained completely at this point, but it may have been due to the formation of solid oxide layer on the electrode. The change in the uncompensated electrolyte resistance with temperature and P_{CO_2} was negligible. The effect of partial pressure of carbon dioxide on log |Z| vs. log ω plot is shown in Fig. 4. The log |Z| vs. log ω plot converged to the value of uncompensated electrolyte resistance at high frequencies. In the low frequency region, complete relaxation due to the charge transfer process was not observed due to the diffusional impedance. Also, it is evident from Fig. 4 that the experimental data concurred with the model data for the entire frequency range of the experiment. Since impedance measurements were obtained at the rest potential, the following expressions can be used for the charge transfer resistance and the Warburg coefficient (28):

$$R_{ct} = \frac{RT}{nFi_o} \qquad [7]$$

$$\sigma = \frac{RT}{n^2F^2A\sqrt{2}}\left(\frac{1}{D_O^{1/2}C_O} + \frac{1}{D_R^{1/2}C_R}\right) \qquad [8]$$

For peroxide reduction in Li_2CO_3 melt, C_O is much smaller than C_R because the final product is carbonate ion. Therefore $1/D_R^{1/2}C_R$ is negligible compared with $1/D_O^{1/2}C_O$. Thus Eqn. [8] can be approximated by the following expression:

$$\sigma = \frac{RT}{n^2F^2A\sqrt{2}}\left(\frac{1}{D_O^{1/2}C_O}\right) \qquad [9]$$

The calculated values of the exchange current density and product, $D_O^{1/2}C_O$, as a function of P_{CO_2} and temperature are given in Tables 1-3. The increase in partial pressure of carbon dioxide, decreased the electrode kinetics, e.g. the exchange current density decreased more than five folds when the partial pressure of carbon dioxide was increased from 0.02 t0 0.4 atm. As shown in Fig. 5, plot

of log i_0 vs. log P_{CO_2} for different temperatures showed a linear behavior and the carbon dioxide reaction order was determined to be about -0.52. As shown in Table 5, the theoretical reaction order is -1.25 when the first charge transfer step (Eqn. [4]) is considered to be the rate determining step and the symmetry factor β is 0.5. The reaction order of the exchange current density with respect to carbon dioxide did not agree with the theoretical reaction order value. This discrepancy in the carbon dioxide reaction order may have been due to slow kinetics of a homogeneous recombination reaction (Eqn. [6]). The Arrhenius plots for the exchange current density are shown in Fig. 6 for different partial pressures of carbon dioxide and the activation energy was calculated to be 131.8 kJ/mol; this value is consistent with the value obtained in the previous work (18). The plots of log $D_O^{1/2}C_O$ vs. log P_{CO_2} for three different temperatures are shown in Fig. 7 and the value of the reaction order with respect to carbon dioxide calculated from these plots is -0.8. As shown in Table 5, the estimated reaction order for peroxide ions agreed well with the theoretical dependence of peroxide concentration on partial pressure of carbon dioxide. The Arrhenius plots for $D_O^{1/2}C_O$ for four partial pressures of carbon dioxide are shown in Fig. 8; the average value of the apparent activation energy was determined to be 185 kJ/mol.

Cyclic Voltammetry

Cyclic voltammetric measurements were made for oxygen reduction on gold electrode in quiescent Li_2CO_3 melt as a function of scan rate, temperature, and P_{CO_2}. The working electrode potential was scanned between the rest potential and -0.5 V vs. the potential of the reference electrode; the scan rate was varied

from 10 to 200 mV/s. The effect of P_{CO_2} on the cyclic voltammogram, recorded at the scan rate of 100 mV/s at 800 °C temperature is shown in Fig. 9. During the forward scan, a diffusion-limited peak followed by a limiting plateau was observed. The peak potential (E_p) was found to be independent of the scan rate (up to 200 mV/s) and the position of this peak corresponded with RT/2F negative to the rest potential, indicating that two electrons are involved in the oxygen reduction in a pure lithium carbonate melt. As shown in Fig. 9, an increase in partial pressure of carbon dioxide, decreased the cathodic peak current density. The current densities in the reverse scan were less cathodic than those obtained in the forward sweep. At the end of the sweep, a large anodic current was observed which subsided slowly and reached zero in a few minutes. This phenomenon is attributed to the local accumulation of the unneutralized oxide ions which shifts the reversible electrode potential in negative direction (29). The effects of P_{CO_2} on the peak current density (i_p) vs. square root of the scan rate ($v^{1/2}$) plot at 800 °C are shown in Fig. 10. A linear behavior of i_p vs. $v^{1/2}$ and invariance of E_p with respect to the scan rate indicate that oxygen reduction in Li_2CO_3 melt is "reversible" up to 200 mV/s (30). An increase in partial pressure of carbon dioxide decreased the slope of i_p vs. $v^{1/2}$ plot, which is directly proportional to $D_O^{1/2}C_O$, where D_O is the diffusion coefficient and C_O is the bulk concentration of the diffusion limiting reactant species. As suggested by Appleby and Nicholson (2), the diffusion-limited peak for O_2 reduction in Li_2CO_3 can be described by the theory developed by Berzins and Delahay (31) for the reversible diffusion controlled peak where the product activity is considered to be invariant and equal to unity (e.g. metal deposition). According to Berzins

and Delahay, the peak current density is given by the following expression:

$$i_p = 0.61(nF/RT)^{1/2} nF D_O^{1/2} C_O^* v^{1/2} \quad [9]$$

The transport parameter, $D_O^{1/2}C_O$, was calculated from the slope of i_p vs. $v^{1/2}$ plot using Eqn. [9]. The calculated values of the transport parameter for various P_{CO_2} and temperatures are compared with those estimated by the electrochemical impedance spectroscopy. An increase in partial pressure of carbon dioxide decreased the product, $D_O^{1/2}C_O$, which is mainly due to the decrease in peroxide ion concentration. Temperature has a significant effect on the product, $D_O^{1/2}C_O$, e.g. for 0.02 atm. partial pressure of carbon dioxide, more than an eight fold increase in $D_O^{1/2}C_O$ was observed when temperature was increased from 750 to 850°C. However, the influence of temperature on $D_O^{1/2}C_O$ was less significant at higher P_{CO_2}. The reaction order and apparent activation energy for $D_O^{1/2}C_O$, estimated by cyclic voltammetry technique concurred with those obtained by impedance analysis.

Conclusions

The kinetic and mass transfer related parameters for the oxygen reduction in pure Li_2CO_3 were determined as a function of P_{CO_2} and temperature by electrochemical impedance spectroscopy and cyclic voltammetry. The impedance spectra were analyzed by the Randles-Ershler equivalent circuit model using a complex nonlinear least square parameter estimation technique. The impedance data analysis determined the electrode kinetic and mass transfer parameters such the charge transfer resistance, Warburg coefficient, double layer capacitance, and uncompensated solution resistance. The influence of carbon dioxide on the Warburg coefficient was examined and the reaction order was estimated to be about

-0.8 which was consistent with the theoretical value of -1.0 for the formation of peroxide species (Eqn. [3]). The diffusion parameters $D_O^{1/2}C_O$ obtained by impedance analysis and by cyclic voltammetry showed an excellent agreement. The effects of partial pressure of carbon dioxide on the electrode kinetics of oxygen reduction showed a decrease in the exchange current density with an increase in partial pressure of carbon dioxide, which is due to the decrease in the concentration of peroxide ions with an increase in the partial pressure of carbon dioxide (Eqn. [3]). The carbon dioxide reaction order for the exchange current density was determined to be -0.52. This value of the reaction order did not agree with the theoretical reaction order of -1.25 for the first charge transfer step (Eqn. [4]) to be the rate determining. This inconsistency in the reaction order may have been due to slow neutralization kinetics (Eqn. [5]), since the partial pressure of carbon dioxide was as low as 0.02 atm. The activation energy for the exchange current density was determined to be about 132 kJ/mol. Also, the reaction order with respect to carbon dioxide and the activation energy for $D_O^{1/2}C_O$ were calculated to be -0.8 and 185 kJ/mol respectively.

The study of diffusion-controlled peak indicated that the oxygen reduction reaction is "reversible" up to 200 mV/s since the peak potential was found to be independent of the scan rate and the peak current density was proportional to the square root of the scan rate. Since the peak potential was observed to be RT/2F negative of the equilibrium potential, the oxygen reduction involved two electron transfer. The carbon dioxide dependence of the diffusion-controlled peak was determined to be -0.8. The dependence of the diffusion-controlled peak on partial pressure of oxygen was determined to be $+0.5$ by cyclic voltammetry and EIS techniques in the previous work (17). These results clearly indicated that

the oxygen reduction reaction on a submerged gold electrode in a pure lithium carbonate is diffusion controlled and the peroxide is the diffusing species. The temperature dependence of the diffusion-controlled peak was also examined and the activation energy was calculated to be about 176.6 kJ mol^{-1}; this activation energy value concurred with that obtained from EIS data.

Acknowledgement

Financial support for this project from the U. S. Department of Energy (Contract No. DE-FG22-87PC79931) and Electric Power Research Institute (Contract No. RP8002-7) is gratefully acknowledged.

List of Symbols

A	electrode area, cm^2
C_{dl}	double layer capacitance, $\mu F/cm^2$
C_j	bulk concentration of species j, mol/cm^3
D_j	bulk diffusion coefficient of species j, cm^2/s
F	Faraday's constant, 96,487 C/equiv.
i	current density, A/cm^2
i_c	charging current density, A/cm^2
i_f	faradaic current density, A/cm^2
i_o	exchange current density, A/cm^2
i_p	peak current density, A/cm^2
n	number of electrons transferred in electrode reaction
P	pressure, atm.
R	universal gas constant, 8.3143 J mol^{-1} K^{-1}
R_{ct}	charge transfer resistance, Ω cm^2
R_s	solution resistance, Ω cm^2
T	temperature, K
v	scan rate, V/s
Z	impedance, Ω cm^2
|Z|	modulus of impedance, Ω cm^2

Greek letters

σ	Warburg coefficient, Ω cm^2 $s^{-1/2}$
ϕ	phase angle
ω	angular frequency, radian/s

Superscripts

$'$	real part
$''$	imaginary part

Subscripts

O	peroxide or superoxide ions
R	carbonate ions

References

1. A. Borucka and C. M. Sugiyama, *Electrochim. Acta*, **13**, 1887, (1968).

2. A. Borucka and C. M. Sugiyama, *Electrochim. Acta*, **14**, 871, (1969).

3. A. J. Appleby and S. B. Nicholson, *J. Electroanal. Chem.*, **38**, App. 14, (1972).

4. A. J. Appleby and S. B. Nicholson, *J. Electroanal. Chem.*, **53**, 105, (1974).

5. A. J. Appleby and S. B. Nicholson, *ibid.*, **83**, 309, (1977).

6. A. J. Appleby and S. B. Nicholson, *ibid.*, **112**, 71, (1980).

7. B. Kr. Andersen, Ph. D. Dissertation, The Technical University of Denmark, Lyngby, Denmark, (1975).

8. A. J. Appleby and C. Van Drunen, *J. Electrochem. Soc.*, **127**, 1655, (1980).

9. W. M. Vogel, S. W. Smith, and L. J. Bregoli, *ibid.*, **130**, 575, (1983).

10. S. W. Smith, W. M. Vogel and S. Kapelner, *ibid.*, **129**, 1668, (1982).

11. G. B. Dunks and D. Stelman, *Inorg. Chem.*, **22**, 2168, (1983).

12. S. H. Lu, Ph. D. Dissertation, Illinois Institute of Technology, Chicago, Il., (1985).

13. I. Uchida, T. Nishina, Y. Mugikura and K. Itaya, *J. Electroanal. Chem.*, **206**, 229, (1986).

14. I. Uchida, T. Nishina, Y. Mugikura and K. Itaya, *ibid.*, **206**, 241, (1986).

15. I. Uchida, T. Nishina, Y. Mugikura and K. Itaya, *ibid.*, **209**, 125, (1986).

16. P. K. Adanuvor, R. E. White and A. J. Appleby, *J. Electrochem. Soc.*, **137**, 2095, (1990).

17. B. B. Dave, R. E. White, S. Srinivasan, and A. J. Appleby, "Electrode Kinetics of Oxygen Reduction in Lithium Carbonate Melt: Use of Impedance Analysis and Cyclic Voltammetry Techniques to Determine the Effects of Partial Pressure of Oxygen," in press *J. Electrochem. Soc.*, (1990).

18. B. B. Dave, R. E. White, S. Srinivasan, and A. J. Appleby, "Impedance Analysis for Oxygen Reduction in a Lithium Carbonate Electrolyte," submitted to *J. Electrochem. Soc.*, (1990).

19. T. Nishina, M. Takahashi, and I. Uchida, *J. Electrochem. Soc.*, **137**, 1112, (1990).

20. R. De Levie and L. Pospísil, *J. Electroanal. Chem.*, **22**, 277, (1969).

21. E. Warburg, *Ann. Phys. Chem.*, **67**, 493, (1899).

22. J. E. B. Randles, *Discuss. Faraday Soc.*, **1**, 11, (1947).

23. B. Ershler, *ibid.*, **1**, 269, (1947).

24. J. R. Macdonald, *J. Electroanal. Chem.*, **223**, 25, (1987).

25. J. R. Macdonald, in "Impedance Spectroscopy -Emphasizing Solid Materials and Systems," J. R. Macdonald, Editor, p. 1, John Wiley & Sons, New York, (1987).

26. J. R. Macdonald, "Impedance Spectroscopy: Old Problems and New Developments," submitted to *Electrochim. Acta*, (August 1990).

27. J. R. Macdonald and L. D. Potter, Jr., *Solid State Ionics*, **23**, 61, (1987).

28. M. Sluyters-Rehbach and J. H. Sluyters, in "Electroanalytical Chemistry," Vol. 4, A. J. Bard, Editor, p. 1, Marcel Dekker, New York, (1970).

29. S. H. Lu and J. R. Selman, *ibid.*, **137**, 1125, (1990).

30. R. S. Nicholson and I. Shain, *Anal. Chem.*, **36**, 706, (1964).

31. T. Berzins and P. Delahay, *J. Amer. Chem. Soc.*, **75**, 555, (1953).

List of Figure Captions

Fig. 1. Phase angle vs. log ω plot as a function of P_{CO_2} for O_2 reduction on gold electrode in Li_2CO_3 melt at 0.6 atm. P_{O_2} and 800°C.

Fig. 2. The Randles-Ershler equivalent circuit model to represent the interfacial impedance for oxygen reduction on gold in lithium carbonate melt.

Fig. 3. Effect of P_{CO_2} on Z' vs. $\omega^{-1/2}$ plot for O_2 reduction on gold electrode in Li_2CO_3 melt at 0.6 atm. P_{O_2} and 800°C; symbols: experimental data; lines: regression data.

Fig. 4. Effect of P_{CO_2} on log |Z| vs. log ω plot for O_2 reduction on gold electrode in Li_2CO_3 melt at 0.6 atm. P_{O_2} and 800°C; symbols: experimental data; lines: regression data.

Fig. 5. Plots of log i_0 vs. log P_{CO_2} for CO_2 reaction orders determination at 0.6 atm. P_{O_2};symbols: experimental data; lines: regression data.

Fig. 6. Plots of log i_0 vs. T^{-1} for determination of activation energy at 0.6 atm. P_{O_2};symbols: experimental data; lines: regression data.

Fig. 7. Plots of log $(D_O^{1/2}C_O)$ vs. log (P_{O_2}) for O_2 reaction orders determination at 0.2 atm. P_{CO_2}; $D_O^{1/2}C_O$ estimated by impedance analysis; symbols: experimental data; lines: regression data.

Fig. 8. Plots of log $(D_O^{1/2}C_O)$ vs. T^{-1} for determination of activation energy at 0.6 atm. P_{O_2}; $D_O^{1/2}C_O$ estimated by impedance analysis. symbols: experimental data; lines: regression data.

Fig. 9. Effect of P_{CO_2} on cyclic voltammogram for O_2 reduction at 0.6 atm. P_{O_2}; reference and working gases have same composition.

Fig. 10. Effect of P_{CO_2} on i_p vs. $v^{1/2}$ plot for O_2 reduction on gold electrode in Li_2CO_3 melt at 0.6 atm. P_{O_2} and 800°C; symbols: experimental data; lines:

regression data.

Table 1. Electrode Kinetic and Mass Transfer Related Parameters Estimated by Electrochemical Impedance Spectroscopic technique at 750 °C Temperature and 0.6 atm. P_{O_2}.

P_{CO_2} atm.	σ $\Omega\ cm^2\ s^{-1/2}$	R_{ct} $\Omega\ cm^2$	$i_0 \times 10^3$ $A\ cm^{-2}$	$C_{dl} \times 10^6$ $F\ cm^{-2}$	R_s $\Omega\ cm^2$
0.02	27.2±0.66	0.53±0.06	86.5±19.3	560.±27.6	0.51
0.04	47.1±0.85	0.66±0.08	70.1±17.2	395.±15.9	0.50
0.08	82.9±2.52	1.07±0.26	43.4±20.5	313.±17.0	0.38
0.20	156.±9.35	2.67±1.03	17.4±13.1	271.±18.5	0.36

Table 2. Electrode Kinetic and Mass Transfer Related Parameters Estimated by Electrochemical Impedance Spectroscopic technique at 800 °C Temperature and 0.6 atm. P_{O_2}.

P_{CO_2} atm.	σ $\Omega\ cm^2\ s^{-1/2}$	R_{ct} $\Omega\ cm^2$	$i_0 \times 10^3$ $A\ cm^{-2}$	$C_{dl} \times 10^6$ $F\ cm^{-2}$	R_s $\Omega\ cm^2$
0.02	10.3±0.34	0.25±0.06	187.±46.2	1250±83.4	0.50
0.04	18.3±0.52	0.42±0.09	111.±24.7	729±41.5	0.53
0.08	31.7±1.06	0.58±0.18	79.4±24.6	509±31.6	0.37
0.20	63.2±1.37	0.84±0.25	55.3±16.8	330.±14.1	0.37
0.40	100.±4.56	1.43±0.91	32.3±20.5	282.±19.3	0.40

Table 3. Electrode Kinetic and Mass Transfer Related Parameters Estimated by Electrochemical Impedance Spectroscopic technique at 850 °C Temperature and 0.6 atm. P_{O_2}.

P_{CO_2} atm.	σ $\Omega\ cm^2\ s^{-1/2}$	R_{ct} $\Omega\ cm^2$	$i_0 \times 10^3$ $A\ cm^{-2}$	$C_{dl} \times 10^6$ $F\ cm^{-2}$	R_s $\Omega\ cm^2$
0.02	4.31±0.16	0.14±0.02	337.±75.1	3220.±225.	0.51
0.04	6.88±0.23	0.18±0.02	265.±62.3	1880.±132.	0.59
0.08	13.3±0.30	0.27±0.03	177.±32.5	891.±48.1	0.39
0.20	27.0±0.57	0.47±0.05	103.±20.1	411.±23.8	0.37
0.40	46.2±1.65	0.71±0.11	67.8±20.3	390..±19.3	0.40

Table 4. Comparison of Product $D_O^{1/2}C_O$ Estimated by Cyclic Voltammetry and Electrochemical Impedance Spectroscopy at 0.2 atm. P_{CO_2}.

	$D_O^{1/2}C_O \times 10^9$ mol cm^{-2} $sec^{-1/2}$					
Temperature °C	750		800		850	
P_{CO_2} atm.	Cyclic Voltammetry	Impedance Analysis	Cyclic Voltammetry	Impedance Analysis	Cyclic Voltammetry	Impedance Analysis
0.02	5.67	5.93±0.15	15.6	16.4±0.54	38.8	41.1±1.48
0.04	3.32	3.43±0.06	9.24	9.25±0.26	24.9	25.8±0.84
0.08	1.92	1.95±0.06	5.07	5.35±0.18	12.6	13.3±0.30
0.20	1.06	1.04±0.07	2.53	2.68±0.06	6.12	6.60±0.14
0.40	0.68		1.55	1.65±0.07	3.61	3.84±0.14

Table 5. The reaction order with respect to carbon dioxide for the exchange current density and $D_O^{1/2}C_O$ estimated by cyclic voltammetric and electrochemical impedance spectroscopic techniques

Parameter	Technique	Temperature °C	Estimated O_2 Reaction Order	Theoretical O_2 Reaction Order
$D_O^{1/2}C_O$	Electrochemical Impedance Spectroscopy	750	−0.77±0.08	−1.00
		800	−0.77±0.04	
		850	−0.80±0.06	
	Cyclic Voltammetry	750	−0.71±0.06	
		800	−0.78±0.05	
		850	−0.81±0.08	
i_0	Electrochemical Impedance Spectroscopy	750	−0.50±0.28	−1.25
		800	−0.55±0.13	
		850	−0.52±0.09	

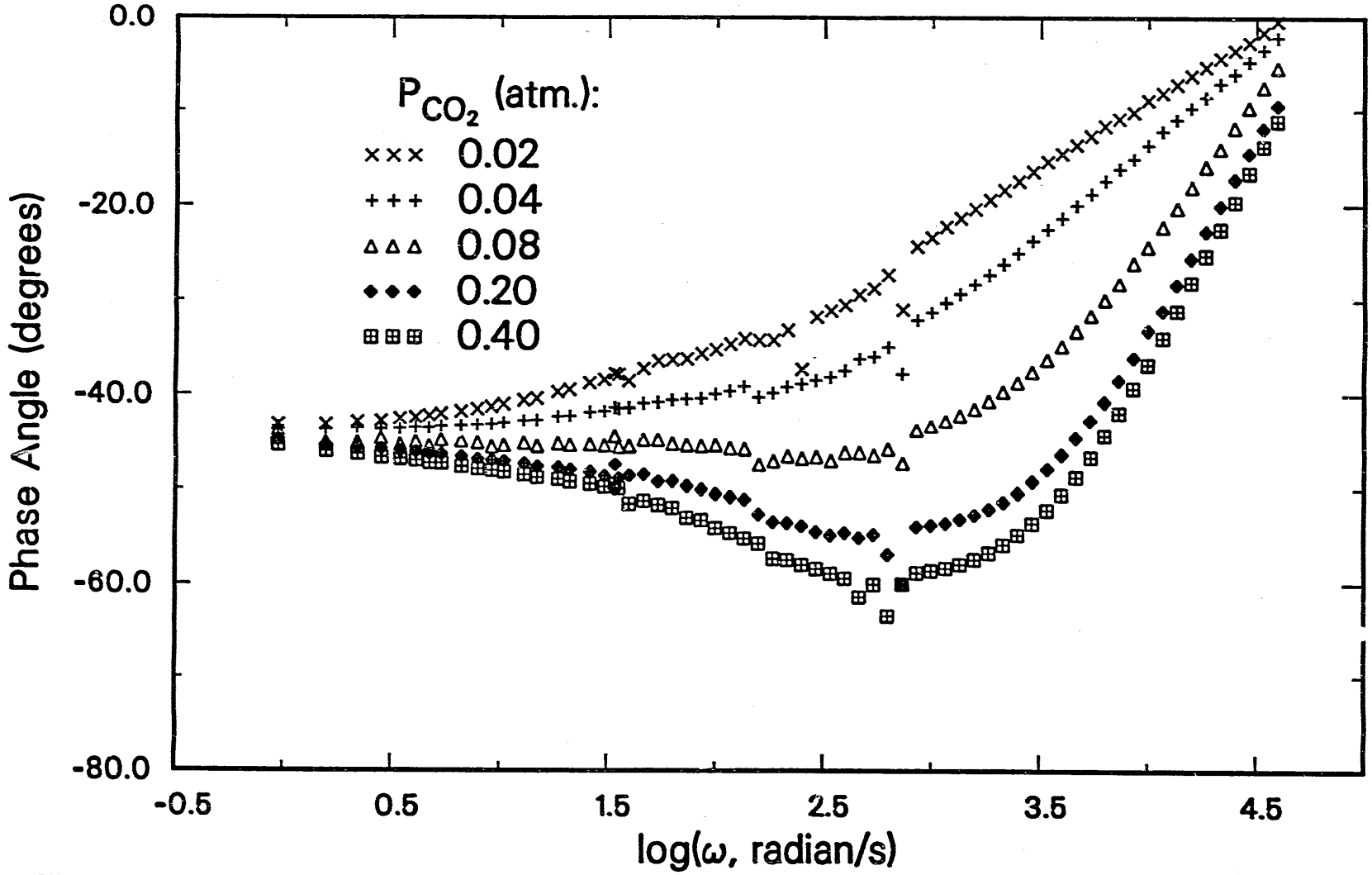

Fig. 1. Phase Angle vs. log ω Plot as a Function of P_{CO_2} for O_2 Reduction on Gold Electrode in Li_2CO_3 Melt at 0.6 atm. P_{O_2} and 800 °C.

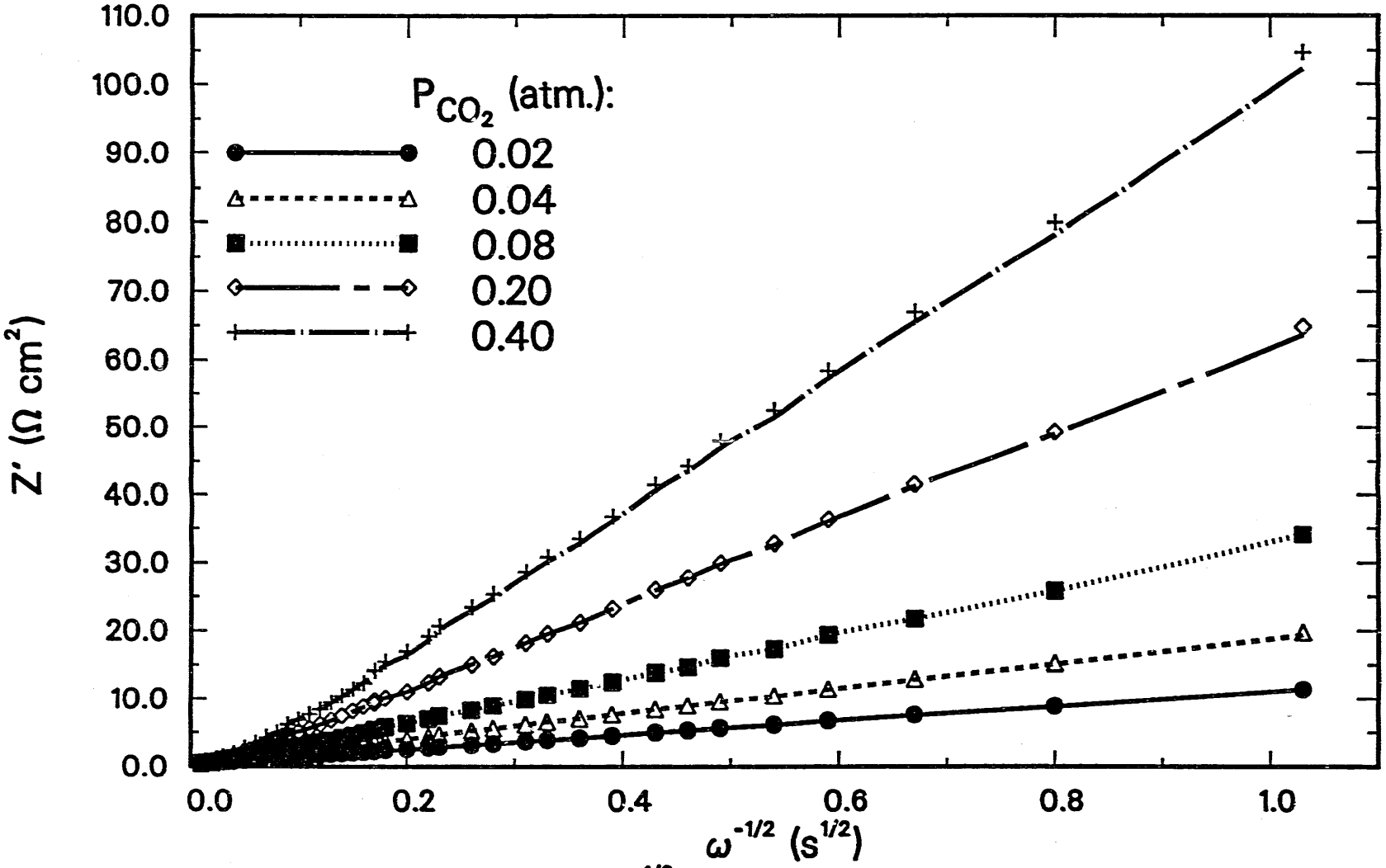

Fig. 3. Effect of P_{CO_2} on Z' vs. $\omega^{-1/2}$ Plot for O_2 Reduction on Gold Electrode in Li_2CO_3 Melt at 0.6 atm P_{O_2} and 800 °C; Symbols: Experimental Data; Lines: Model Data.

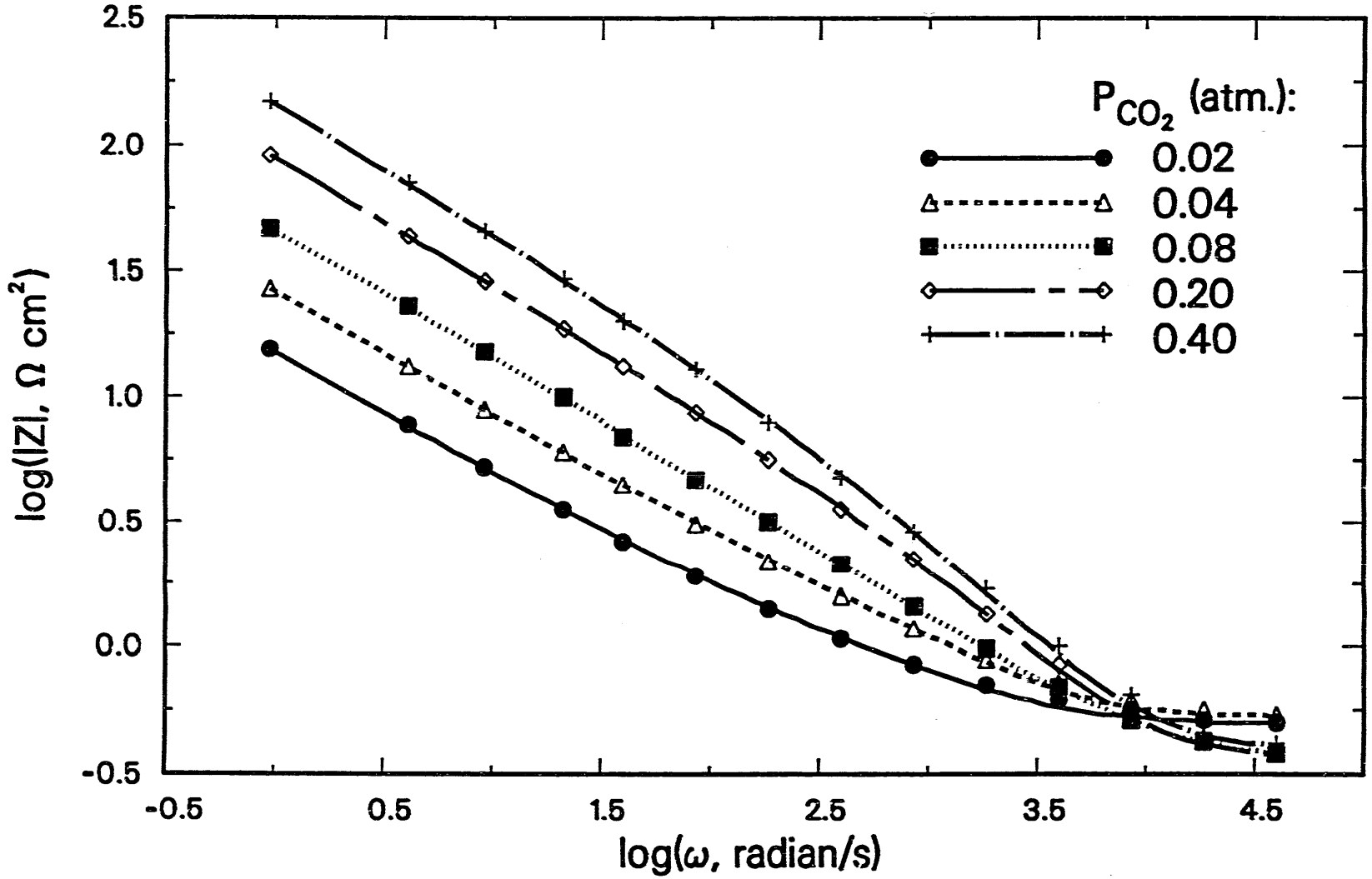

Fig. 4. Effect of P_{CO_2} on log |Z| vs. log ω Plot for O_2 Reduction on Gold Electrode in Li_2CO_3 Melt at 0.6 atm P_{O_2} and 800 °C; Symbols: Experimental data; Lines: Model Data.

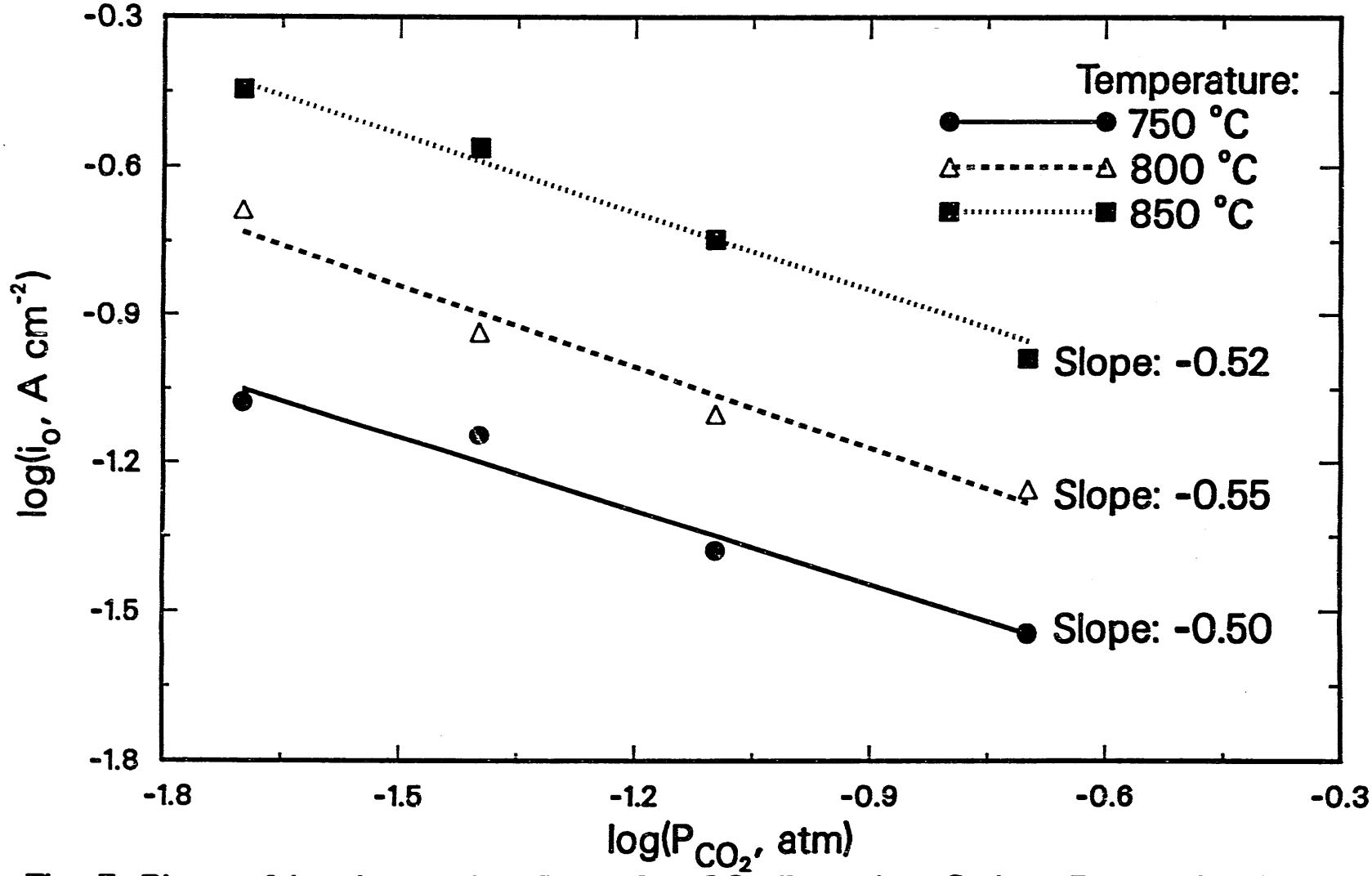

Fig. 5. Plots of log i_o vs. log P_{CO_2} for CO_2 Reaction Orders Determination at 0.6 atm P_{O_2}; Symbols: Experimental Data; Lines: Regression Data.

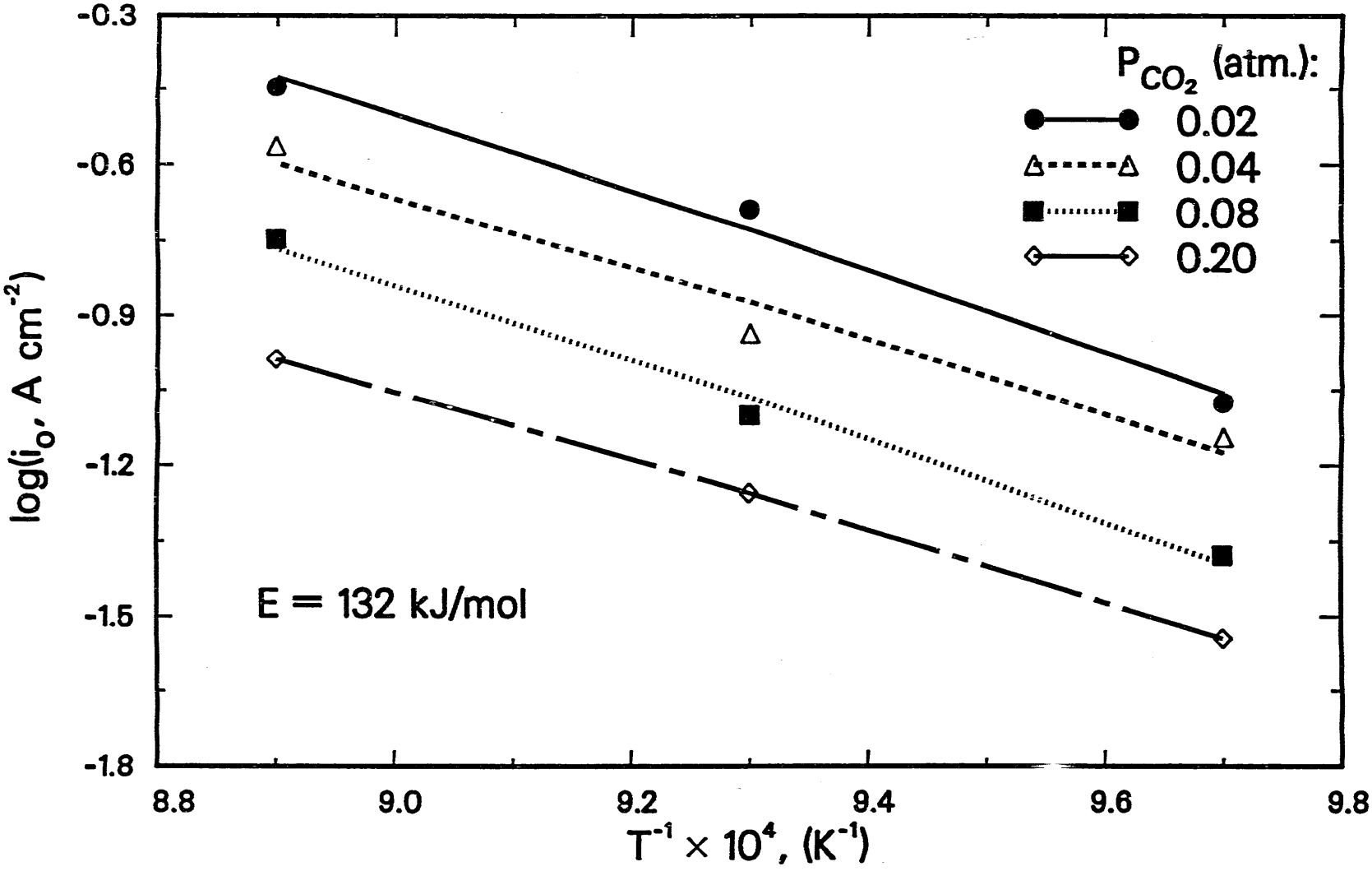

Fig. 6. Plots of log i_o vs. T^{-1} for Activation Energies Determination at 0.6 atm. P_{O_2}; Symbols: Experimental Data; Lines: Regression Data.

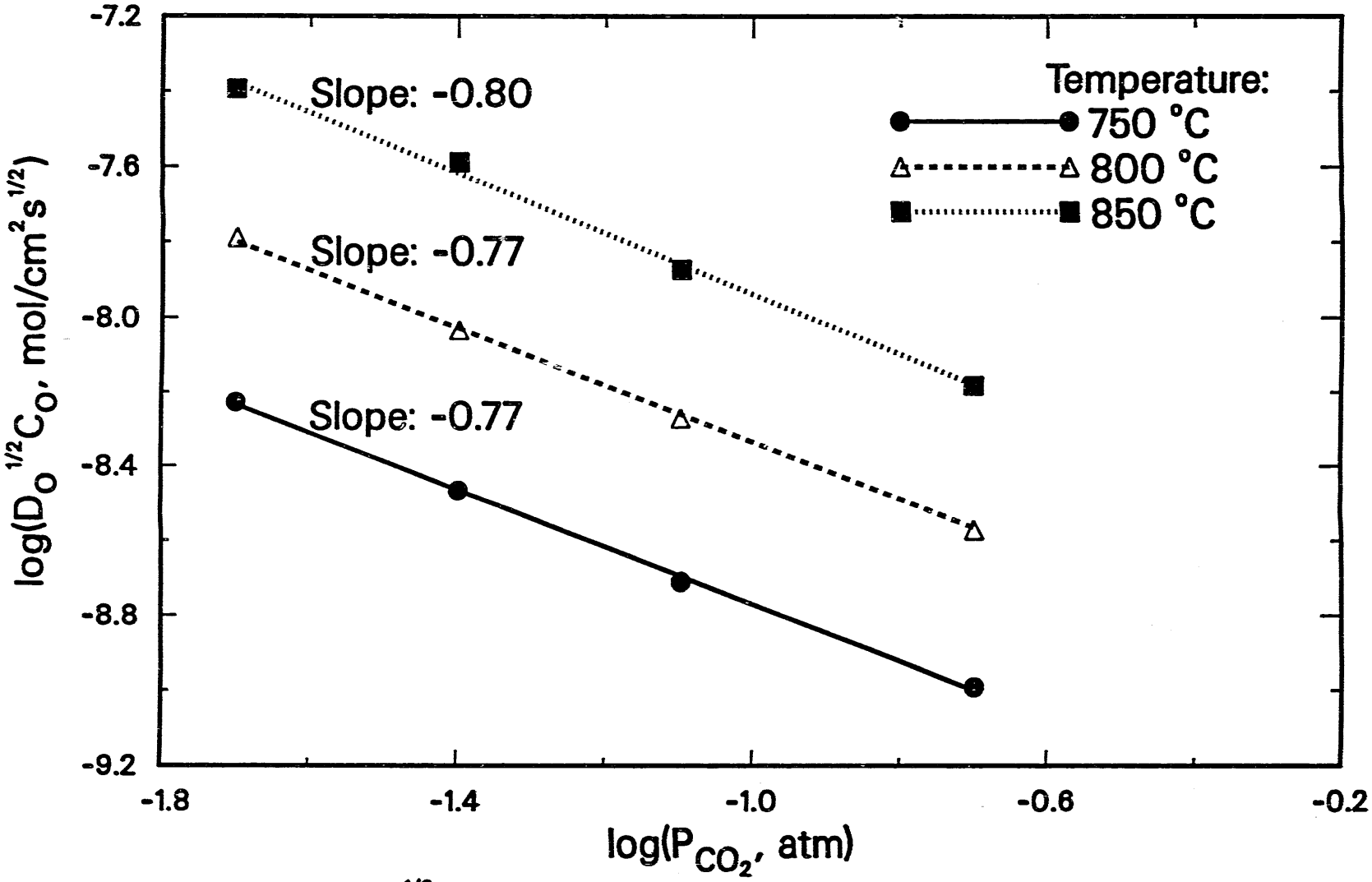

Fig. 7. Plots of log $D_O^{1/2}C_O$ vs. log P_{CO_2} for Determination of CO_2 Reaction Orders at 0.6 atm P_{O_2}; $D_O^{1/2}C_O$ Obtained by Impedance Analysis.

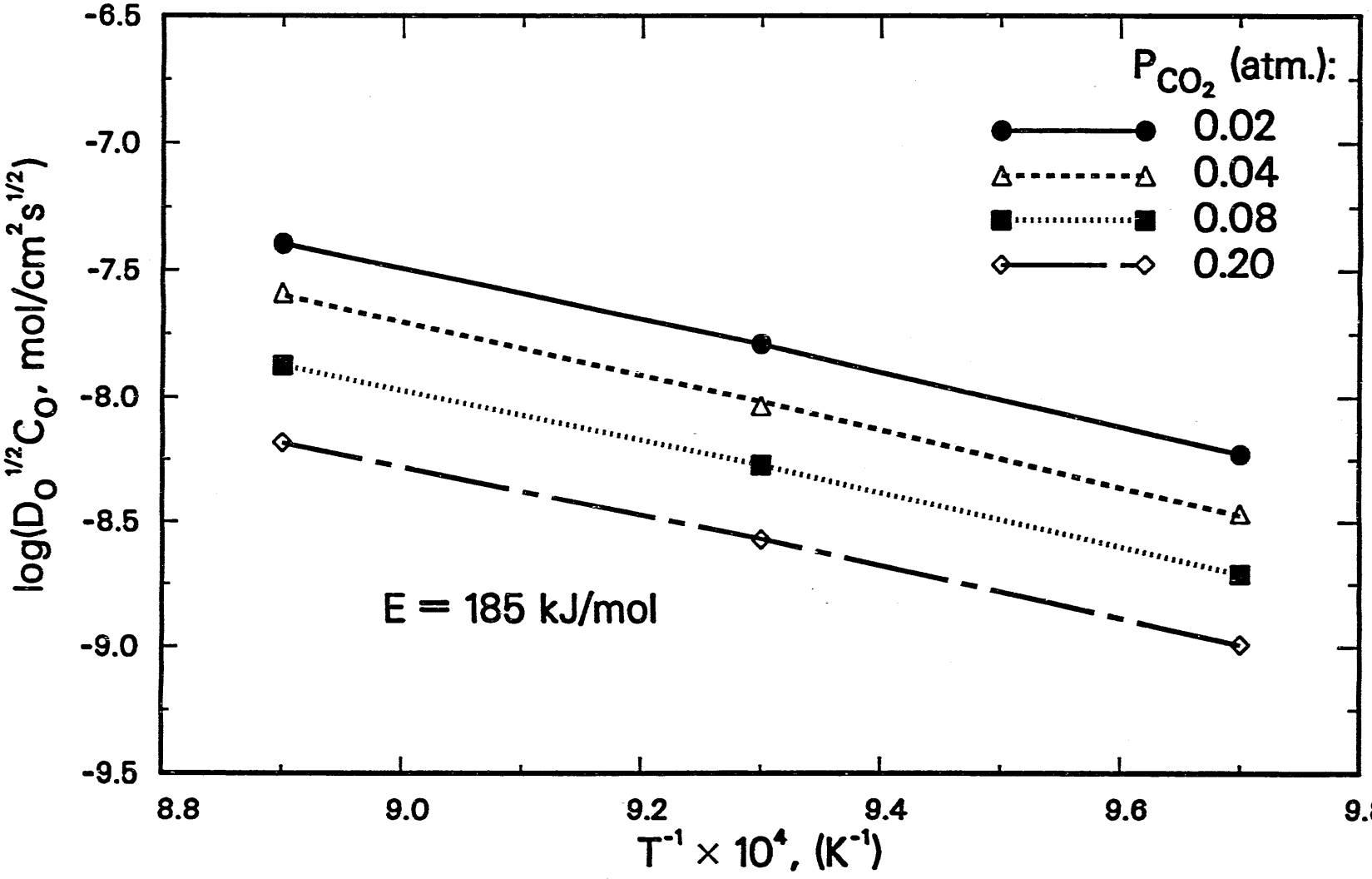

Fig. 8. Plots of log $D_O^{1/2}C_O$ vs. T^{-1} for Activation Energies Determination at 0.6 atm P_{O_2}; $D_O^{1/2}C_O$ Obtained by Impedance Analysis.

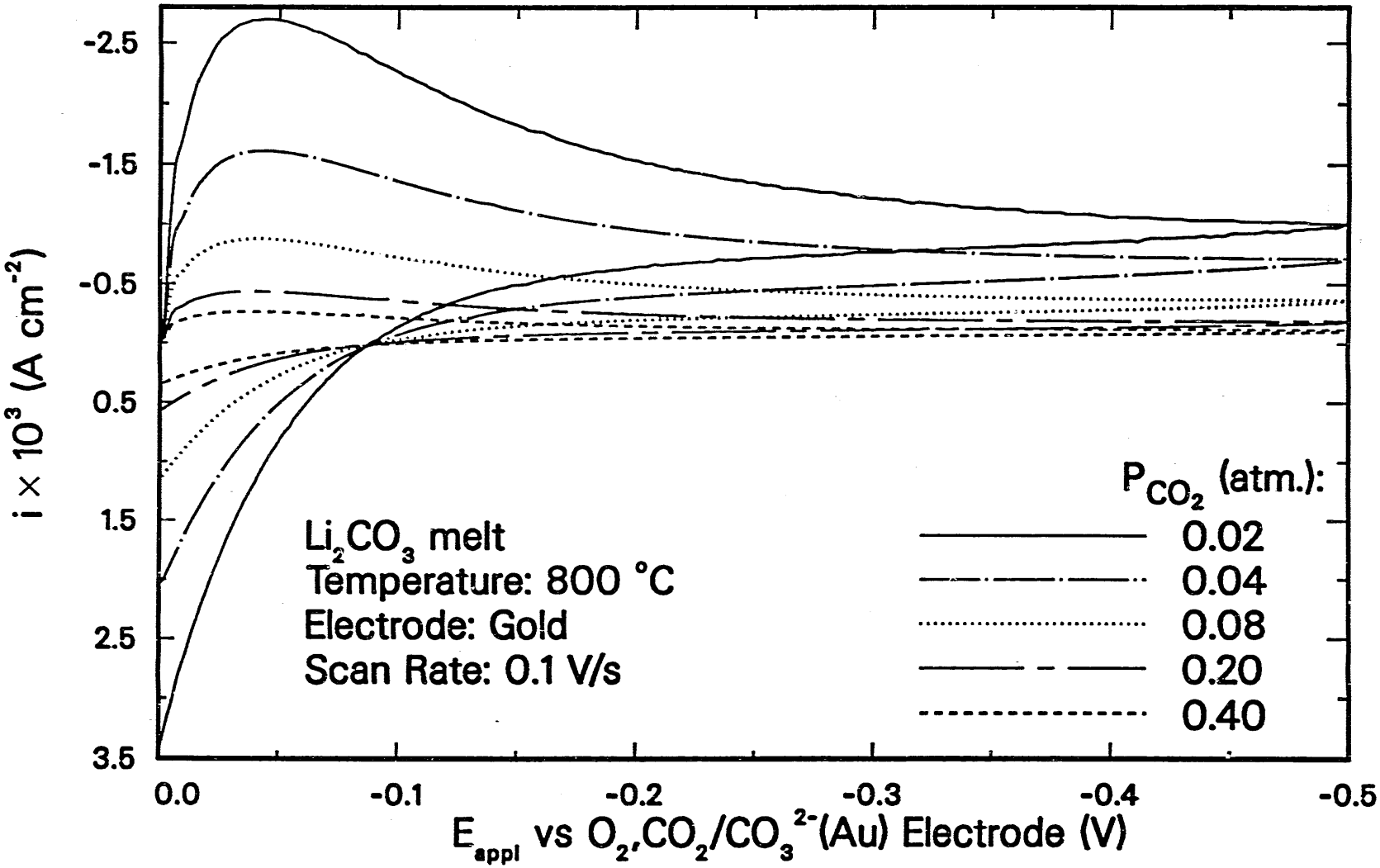

Fig. 9. Effect of P_{CO_2} on Cyclic Voltammogram for O_2 Reduction at 0.6 atm. P_{O_2}; Reference and Working Gases Have Same Composition.

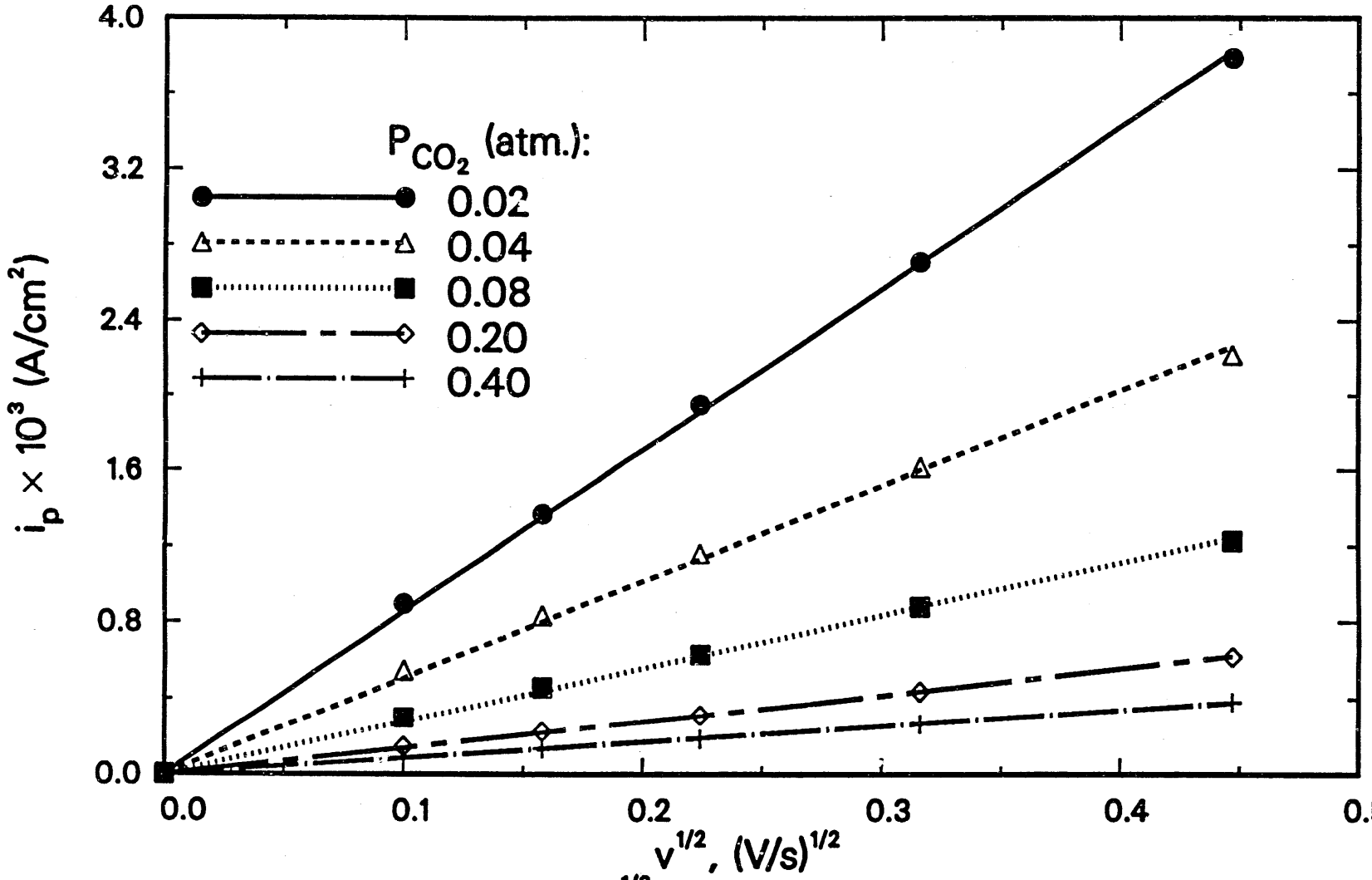

Fig. 10. Effect of P_{CO_2} on i_p vs. $v^{1/2}$ Plot for O_2 Reduction on Gold Electrode in Li_2CO_3 Melt at 0.6 atm. P_{O_2} and 800 °C.

END

DATE FILMED

03/01/91